Zinc Oxide Nanowires

Low-Temperature Wafer-Scale Production of ZnO Nanowire Arrays**

*Lori E. Greene, Matt Law, Joshua Goldberger, Franklin Kim, Justin C. Johnson, Yanfeng Zhang, Richard J. Saykally, and Peidong Yang**

Since the first report of ultraviolet lasing from ZnO nanowires,[1] substantial effort has been devoted to the development of synthetic methodologies for one-dimensional ZnO nanostructures. Among the various techniques described in the literature, evaporation and condensation processes are favored for their simplicity and high-quality products, but these gas-phase approaches generally require economically prohibitive temperatures of 800–900 °C.[2] Despite recent MOCVD schemes that reduced the deposition temperature to 450 °C by using organometallic zinc precursors,[3] the commercial potential of gas-phase-grown ZnO nanowires remains constrained by the expensive and/or insulating (for example, Al_2O_3) substrates required for oriented growth, as well as the size and cost of the vapor deposition systems. A low-temperature, large-scale, and versatile synthetic process is needed before ZnO nanowire arrays find realistic applications in solar energy conversion, light emission, and other promising areas.

Solution approaches to ZnO nanowires are appealing because of their low growth temperatures and good potential for scale-up. In this regard, Vayssieres et al. developed a hydrothermal process for producing arrays of ZnO microrods and nanorods on conducting glass substrates at 95 °C.[4,5] Recently, a seeded growth process was used to make helical ZnO rods and columns at a similar temperature.[6] Here we expand on these synthetic methods to produce homogeneous and dense arrays of ZnO nanowires that can be grown on arbitrary substrates under mild aqueous conditions. We present data for arrays on four-inch (ca. 10 cm) silicon wafers and two-inch plastic substrates, which demonstrate the ease of commercial scale-up. The simple two-step procedure yields oriented nanowire films with the largest surface area yet reported for nanowire arrays. The growth process ensures that a majority of the nanowires in the array are in direct contact with the substrate and provide a continuous pathway for carrier transport, an important feature for future electronic devices based on these materials.

Well-aligned ZnO nanowire arrays were grown using a simple two-step process. In the first step, ZnO nanocrystals (5–10 nm in diameter) were spin-cast several times onto a four-inch Si(100) wafer to form a 50–200-nm thick film of crystal seeds. Between coatings, the wafer was annealed at 150 °C to ensure particle adhesion to the wafer surface. The ZnO nanocrystals were prepared according to the method of Pacholski.[7] A NaOH solution in methanol (0.03 M) was added slowly to a solution of zinc acetate dihydrate (0.01 M) in methanol at 60 °C and stirred for two hours. The resulting nanoparticles are spherical and stable for at least two weeks in solution. After uniformly coating the silicon wafer with ZnO nanocrystals, hydrothermal ZnO growth was carried out by suspending the wafer upside-down in an open crystallizing dish filled with an aqueous solution of zinc nitrate hydrate (0.025 M) and methenamine or diethylenetriamine (0.025 M) at 90 °C. Reaction times spanned from 0.5 to 6 h. The wafer was then removed from solution, rinsed with deionized water, and dried. A field-emission scanning electron microscope (FESEM) was used to examine the morphology of the nanowire array across the entire wafer, while single nanowires were characterized by transmission electron microscopy (TEM). Nanowire crystallinity and growth direction were analyzed by X-ray diffraction and electron diffraction techniques.

SEM images taken of several four-inch samples showed that the entire wafer was coated with a highly uniform and densely packed array of ZnO nanowires (Figure 1). X-ray diffraction (not shown) gave a wurtzite ZnO pattern with an enhanced (002) peak resulting from the vertical orientation of the nanowires. A typical synthesis (1.5 h) yielded wires with diameters ranging between 40–80 nm and lengths of 1.5–2 μm.

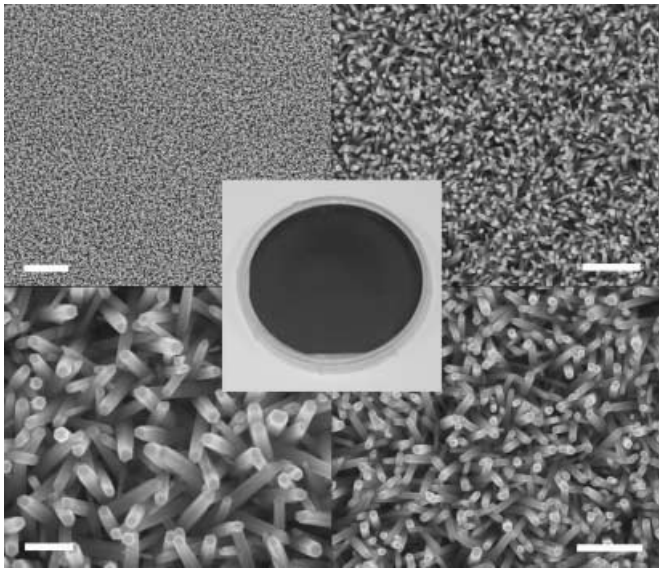

Figure 1. ZnO nanowire array on a four-inch (ca. 10 cm) silicon wafer. At the center is a photograph of a coated wafer, surrounded by SEM images of the array at different locations and magnifications. These images are representative of the entire surface. Scale bars, clockwise from upper left: 2 μm, 1 μm. 500 nm, and 200 nm.

[*] Prof. P. Yang, L. E. Greene,[+] M. Law,[+] J. Goldberger, F. Kim, J. C. Johnson, Y. Zhang, Prof. R. J. Saykally
Department of Chemistry
Lawrence Berkeley National Laboratory
University of California, Berkeley, CA 94720 (USA)
E-mail: p_yang@uclink.berkeley.edu

[+] These authors have contributed equally to this work.

[**] This work was supported by the Department of Energy. P.Y. is an Alfred P. Sloan Research Fellow. Work at the Lawrence Berkeley National Laboratory was supported by the Office of Science, Basic Energy Sciences, Division of Materials Science of the U.S. Department of Energy. We thank the National Center for Electron Microscopy for the use of their facilities.

 DOI: 10.1002/anie.200351461

With a measured nanowire number density on the order of 10^{10} cm^{-2}, these arrays have a ZnO surface area of, conservatively, at least 50 cm^2 per cm^2 of substrate (~ 10 m^2 g^{-1}). The average size of the nanowires increased with longer reaction time, up to 200–300 nm wide by 3 μm long for a 6-h experiment (Figure 2a). High-magnification SEM imaging of a sample grown for 6 h (Figure 2b) reveals that the surfaces of these solution-grown wires are rough compared to the gas-phase nanowire arrays produced in our laboratory, which might be expected for crystallization in a solution environment. Also, a substantial percentage of the nanowires fuse together after longer reaction times.

Cross-sectional SEM views of the arrays (Figure 2c) suggest that the ZnO nanowires grow nearly vertically and penetrate a thin (~ 100 nm) layer of nanocrystals. It is desirable for electronic applications to make the nanoparticle layer as thin and continuous as possible, ideally a few particle diameters in extent. No effort has been made here to optimize the deposition of the nanoparticle film. In the future, improved nanoparticle spin-coating or Langmuir–Blodgett techniques will be used to address this issue.

TEM characterization of individual nanowires removed from the arrays indicates that they are single-crystalline and grow in the [0001] direction (Figure 2d). The cluster morphology shown in the image is fairly common and suggests that multiple nanowires often grow from a single aggregate of ZnO nanoparticles attached to the substrate. We would like to point out that the initial deposition of the nanocrystals is critical for the formation of the current arrays of nanowires with thin diameters. Otherwise, microrod arrays would be obtained, as has been reported earlier.[4] Further investigation is needed to better understand the detailed mechanism of this nanowire growth process. In addition, unlike previous reports[4] where crystal growth occurs within enclosed flasks, the current process is carried out in open vessels, which points to the possibility of large-scale reel-to-reel production of such nanowire arrays.

This low-temperature hydrothermal method is substrate-independent and produces high-quality nanowire arrays on ITO glass, sapphire, titanium foil, and polymer surfaces. Figure 3 shows the growth of a nanowire array on a flexible two-inch polydimethylsiloxane (PDMS) substrate. This array is identical to those grown on silicon except for a network of microscale cracks (Figure 3c) that form because of the inflexibility of the ZnO nanowire film.

The ultraviolet and visible photoluminescence (PL) of as-grown nanowire arrays was measured in the temperature range $4.5 \leq T \leq 300$ K using a low-power, unfocused 325 nm

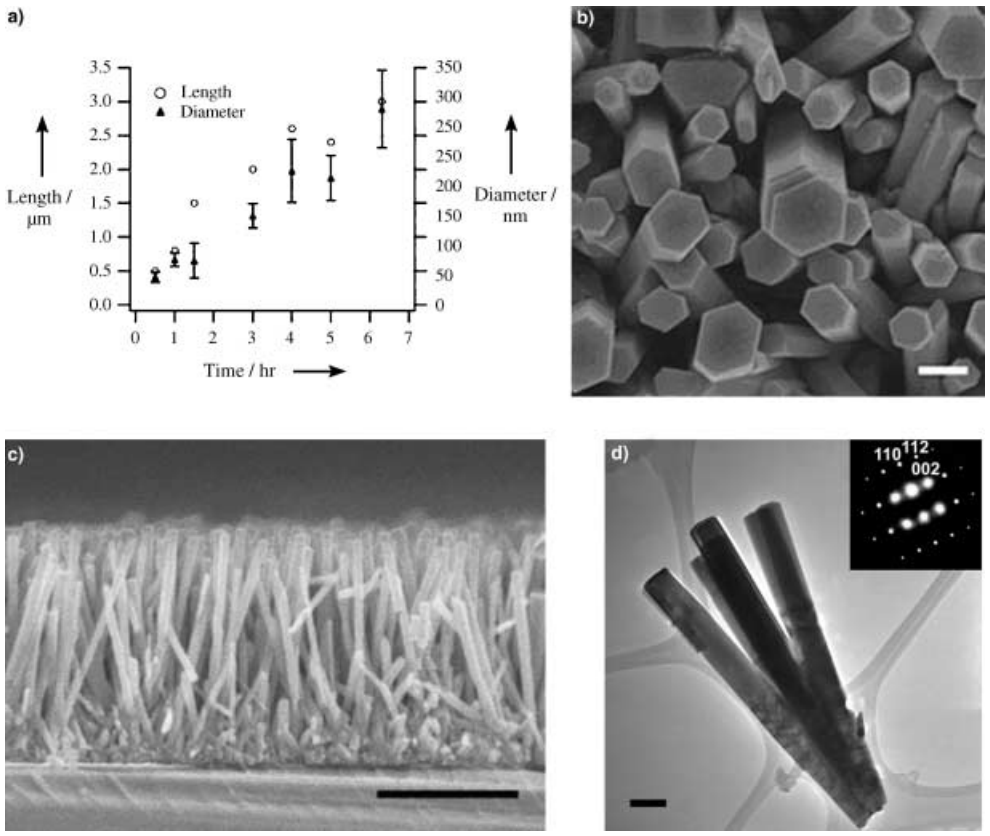

Figure 2. a) Plot showing the average length and diameter of array nanowires as a function of growth time. Each diameter data point was determined using 100 nanowires, with error bars indicating the standard deviation; b) SEM image of an array grown over 6 h showing the relatively rough surfaces of the nanowires (scale bar = 200 nm); c) cross-sectional SEM image of an array grown over 1.5 h on a silicon wafer (scale bar = 1 μm); d) transmission electron micrograph of a cluster of ZnO nanowires removed from an array grown over 1.5 h (scale bar = 90 nm). The inset shows the [100] electron diffraction pattern of an isolated, single nanowire from a different region of the sample. The growth axis is along the [001] direction.

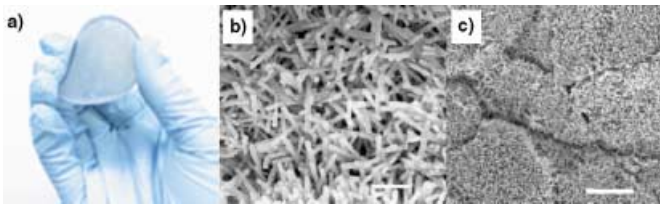

Figure 3. ZnO nanowire array on a two-inch (ca. 5 cm) PDMS substrate. a) Photograph of the flexed array on PDMS; b) SEM image showing the array morphology (scale bar = 1 μm); c) Low-magnification SEM image of the cracks formed in the array after handling (scale bar = 5 μm).

line of a He–Cd laser as the excitation source. Room-temperature spectra of as-grown samples show a weak band-edge emission at 378 nm (3.29 eV) resulting from free-exciton annihilation, and a very strong and broad yellow-orange emission that is fit well by two Gaussians, with a major peak centered at 605 nm (2.05 eV) and a shoulder at 730 nm (1.70 eV). The three peaks grow more intense with decreasing temperature as a result of the freeze-out of phonons and quenching of nonradiative recombination processes (Figure 4). A 90 meV blue shift of the band-edge emission over this temperature range (Figure 4 inset) is caused by the thermal contraction of the lattice and changing electron–phonon interactions.[8] The temperature dependence of the orange (2.05 eV) PL intensity can be expressed by a simple thermal activation model of the form,[9]

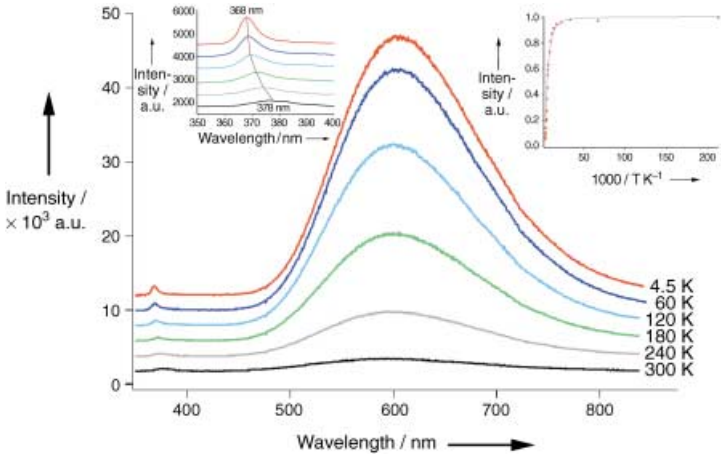

Figure 4. Temperature-dependent photoluminescence of a ZnO nanowire array on a silicon substrate; spectra are offset for clarity. The left inset is a magnification of the band-edge emission showing a 90 meV blue shift (3.29 to 3.38 eV) as the temperature was lowered from 300 to 4.5 K. The right inset is the normalized intensity of the orange emission plotted as a function of inverse temperature. The solid line is a theoretical fit to the data as described in the text.

$$I = I_O/(1 + A\exp(-E_A/k_B T)). \quad (1)$$

By fitting the experimental data (Figure 4 inset) we obtain an activation energy $E_A = 71$ meV for the nonradiative mechanisms responsible for quenching the orange luminescence. This value is comparable to the energy reported in a previous study of single-crystal and powder samples.[10]

It is known that pure ZnO can show green and/or orange visible luminescence depending on the growth temperature and availability of oxygen during sample preparation.[11] The green emission results from the recombination of electrons with holes trapped in singly ionized oxygen vacancies (V_O^+) and is commonly seen in ZnO materials synthesized under oxygen-deficient conditions, such as the gas-phase nanowires produced in this laboratory.[12] The orange emission is less commonly reported and its origin, although not fully understood, seems to involve interstitial oxygen ions (O_i^-).[13] Orange PL has been seen in ZnO grown electrochemically,[14] hydrothermally,[15] and by pulsed laser deposition[16] and spray pyrolysis.[17] The strong orange PL and complete absence of green emission from the nanowire arrays grown under aqueous conditions presented in this work is consistent with the above assignments. Regardless of the exact origin of the orange emission, the large ratio of orange PL intensity to band-edge PL intensity indicates that the as-grown nanowires are rich in atomic defects.

PL and lasing measurements were combined with a series of annealing treatments to investigate the nature of the orange emission. Three samples were collected from arrays prepared in both 1.5-h and 3-h experiments on silicon, and then annealed in one of three environments; either 400 °C in 10 % H_2/90 % Ar for 15 min, 500 °C in 10 % H_2/90 % Ar for 15 min, or 800 °C at 5×10^{-6} Torr for 2 h. One sample from each wafer was left untreated as a control. Post-anneal SEM imaging of each sample confirmed that the nanowires survived visibly undamaged, except for a slight surface etching seen in the 500 °C H_2 treatments. Room-temperature PL spectra of samples prepared over 1.5 h show a progressive quenching of the orange emission with a simultaneous increase of the band-edge PL intensity (Figure 5). The marked weakening of the orange emission after vacuum annealing is consistent with the involvement of oxygen interstitials in the luminescence. The 500 °C H_2 treatment causes a nearly complete quenching of the orange PL and results in a spectrum that is dominated by band-edge emission. It is interesting that the green PL feature, which should develop in response to sufficiently reducing treatments,[17] was not observed even in an array sample that was exposed to hydrogen at 600 °C and appeared heavily etched in SEM.

The lasing behavior of the eight array samples was investigated by far-field PL imaging using an experimental setup described previously.[18] We found that neither of the as-grown samples showed lasing at sub-ablation pumping intensities. Lasing of array nanowires on the annealed 1.5-h samples was observed in only a small fraction of the wires, most likely those at the upper limit of the diameter distribution, which have a sufficient cavity finesse to support a single lasing mode. The annealed 3-h samples (average diameter $d = 125$ nm, length 2 μm) showed lasing in roughly ten times the number of wires as the 1.5-h arrays (average diameter 60 nm, length 1.5 μm), which is reasonable

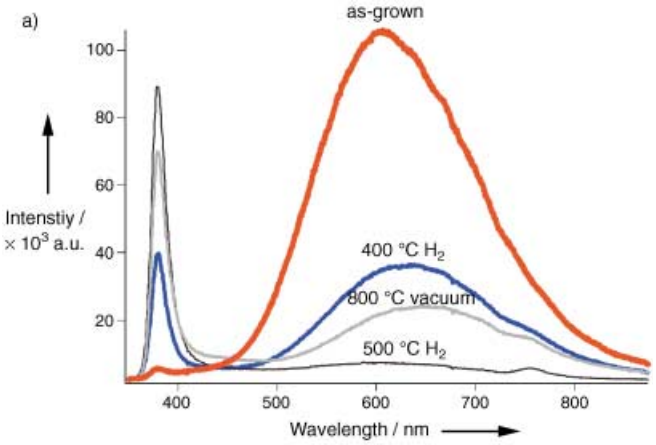

c)

Sample	Treatment	Threshold / μJ cm^{-2}
3-hour solution no.1	none	> 15
3-hour solution no.2	800°C vacuum	6.1
3-hour solution no.3	400°C H_2 / Ar	3.9
3-hour solution no.4	500°C H_2 / Ar	2.9
Gas phase	none	0.50

Figure 5. Photoluminescence spectra of four arrays (a) grown over 1.5 h after annealing treatments. Samples prepared over 3 h (b) showed qualitatively identical behavior; (c) Average lasing thresholds for active wires.

as less diffraction loss would be expected for larger wires. A typical PL spectrum of a solution array prepared over 3 h and pumped above threshold (Figure 5b) shows several relatively sharp lasing peaks superimposed on a broad PL background. However, the percentage of lasing wires in the 3-h arrays remained low, probably because their short wire lengths lead to high gain thresholds. A comparison of the average lasing thresholds for the active wires on the three annealed solution-grown arrays and a gas-phase array (Figure 5c) illustrates that the threshold tends to decrease as the ratio of ultraviolet PL to visible PL increases, with the gas-phase array lasing at one fifth of the threshold of the most reduced 3-h sample. A more detailed analysis of the optical properties of the various ZnO nanowire arrays is forthcoming.

Dense arrays of ZnO nanowires with high surface area can be grown on arbitrary substrates of any size using the mild solution process described in this study. The use of small, homogeneous ZnO nanocrystals as a seed layer helps produce nanowires of relatively small diameter. The nanowires are well-oriented and most are in intimate contact with the substrate. Annealing as-grown arrays in reducing atmospheres quenches the intense orange emission and lowers the lasing threshold of the larger nanowires to values similar to gas-phase samples. With further improvements, these ZnO nanowire arrays should find applications in solar cells, light emission, and other devices.

Received: March 24, 2003 [Z51461]

Keywords: electron microscopy · nanowires · oxides · photoluminescence · zinc

[1] a) M. H. Huang, S. Mao, H. Feick, H. Yan, Y. Wu, H. Kind, E. Weber, R. Russo, P. Yang, *Science* **2001**, *292*, 1897; b) J. Johnson, H. Yan, R. Schaller, L. Haber, R. Saykally, P. Yang, *J. Phys. Chem. B* **2001**, *105*, 11387.
[2] a) P. Yang, H. Yan, S. Mao, R. Russo, J. Johnson, R. Saykally, N. Morris, J. Pham, R. He, H. Choi, *Adv. Funct. Mater.* **2002**, *12*, 323; b) B. D. Yao, Y. F. Chan, N. Wang, *Appl. Phys. Lett.* **2002**, *81*, 757.
[3] W. I. Park, G. Yi, M. Kim, S. L. Pennycook, *Adv. Mater.* **2002**, *14*, 1841.
[4] L. Vayssieres, K. Keis, A. Hagfeldt, S. Lindquist, *Chem. Mater.* **2001**, *13*, 4395.
[5] L. Vayssieres, *Adv. Mater.* **2003**, *15*, 464.
[6] Z. R. Tian, J. A. Voigt, J. Liu, B. Mckenzie, M. J. Mcdermott, *J. Am. Chem. Soc.* **2002**, *124*, 12954.
[7] C. Pacholski, A. Kornowski, H. Weller, *Angew. Chem.* **2002**, *114*, 1234; *Angew. Chem. Int. Ed.* **2002**, *41*, 1188.
[8] X. T. Zhang, Y. C. Liu, Z. Z. Zhi, J. Y. Zhang, Y. M. Lu, D. Z. Shen, W. Xu, X. W. Fan, X. G. Kong, *J. Lumin.* **2002**, *99*, 149.
[9] D. S. Jiang, H. Jung, K. Ploog, *J. Appl. Phys.* **1988**, *64*, 1371.
[10] R. B. Lauer, *J. Phys. Chem. Solids* **1973**, *34*, 249.
[11] a) Y. Zelikin, A. P. Zhukovskii, *Opt. Spektrosk.* **1961**, *11*, 397; b) S. Bhushan, R. P. Asare, *Indian J. Pure Appl. Phys.* **1981**, *19*, 694.
[12] A. van Dijken, E. A. Meulenkamp, D. Vanmaekelbergh, A. Meijerink, *J. Lumin.* **2000**, *90*, 123.
[13] M. Liu, A. H. Kitai, P. Mascher, *J. Lumin.* **1992**, *54*, 35.
[14] M. J. Zheng, L. D. Zhang, G. H. Li, W. Z. Shen, *Chem. Phys. Lett.* **2002**, *363*, 123.
[15] T. Sekiguchi, S. Miyashita, K. Obara, T. Shishido, N. Sakagami, *J. Cryst. Growth* **2000**, *214*/215, 72.
[16] X. L. Wu, G. G. Siu, C. L. Fu, H. C. Ong, *Appl. Phys. Lett.* **2001**, *78*, 2285.
[17] S. A. Studenikin, N. Golego, M. Cocivera, *J. Appl. Phys.* **1998**, *84*, 2287.
[18] a) J. Johnson, H. J. Choi, K. P. Knutsen, R. D. Schaller, P. Yang, R. J. Saykally, *Nat. Mater.* **2002**, *1*, 101; c) H. Yan, R. He, M. Law, J. Johnson, R. Saykally, P. Yang, *J. Am. Chem. Soc.* **2003**, *125*, 4728.

